A density functional tight-binding approach for modelling Ge and GeH structures

1996 J. Phys.: Condens. Matter 8 6873

(http://iopscience.iop.org/0953-8984/8/37/009)

J. Phys.: Condens. Matter **8** (1996) 6873–6888. Printed in the UK

A density functional tight-binding approach for modelling Ge and GeH structures

P K Sitch†, Th Frauenheim† and R Jones‡

† Institut für Physik, Technische Universität, Chemnitz, D-09127, Germany

‡ Department of Physics, University of Exeter, Exeter EX4 4QL, UK

Received 25 March 1996, in final form 15 May 1996

Abstract. We present here details of a density-functional-based non-orthogonal tight-binding approach for germanium. This is carried out within the framework of the LCAO *ansatz*, using a two-centre approximation for the evaluation of the Hamiltonian matrix elements. The Hamiltonian and overlap matrix elements for Ge–Ge, Ge–H are derived using a localized atomic basis set and existing parameters for H–H are utilized. These are tested against results from existing experimental and theoretical data for bulk germanium and germanium surface reconstructions, both with and without hydrogen. In addition we generate the first fully self-consistent *ab initio* LDA results for small Ge clusters and Ge–H molecules using the AIMPRO program and compare DF-TB results against these. Finally we describe our study of H point defects in bulk germanium. These are the first calculations of this type done on Ge using large fully optimized supercells and confirm self-consistent *ab initio* calculations done on small clusters. We consequently demonstrate that, despite the extreme simplicity of the approach, it is accurate and highly transferable across a broad range of structural systems ranging from clusters to the bulk phase.

1. Introduction

Germanium is a particularly interesting material as it has been found to exist in a wide range of condensed phases, each with complex electrical and structural properties. In its crystalline form it is a semiconductor with the diamond lattice structure, a narrow indirect band gap of 0.74 eV and bond length 2.45 Å. A semiconductor–metal transition is found to occur at high pressure, with the Ge structure changing to that of β-tin. Two further semiconducting metastable phases, ST12 and BC8, can be observed on releasing the pressure from the β-tin phase [1, 2]. In the liquid state, Ge is metallic with a larger density than that of the crystalline form. A molecular dynamics (MD) scheme using *ab initio* approaches [3, 4] has been used to investigate this phase. There is also much interest in amorphous germanium, a-Ge. This forms a continuous random network (CRN) of mostly fourfold-coordinated atoms, together with some defects. An MD empirical potential approach has been used to investigate this by Ding and Andersen [5]. Furthermore, the high quality of current hydrogenated germanium (a-Ge:H) films suggests the possibility of applications in solar cell technology [6].

The expense of self-consistent calculations and the lack of transferability of empirical potentials in a material with such a broad range of possible structures imply that our density-functional-based tight-binding (henceforth referred to as DF-TB) method is the ideal tool for investigating the various condensed matter phases of germanium. This method has been successfully applied to carbon [7], silicon [8] and boron nitride [9] where it has proved to be fast, accurate and able to account for a broad range of cluster and solid-state phenomena.

0953-8984/96/376873+16$19.50

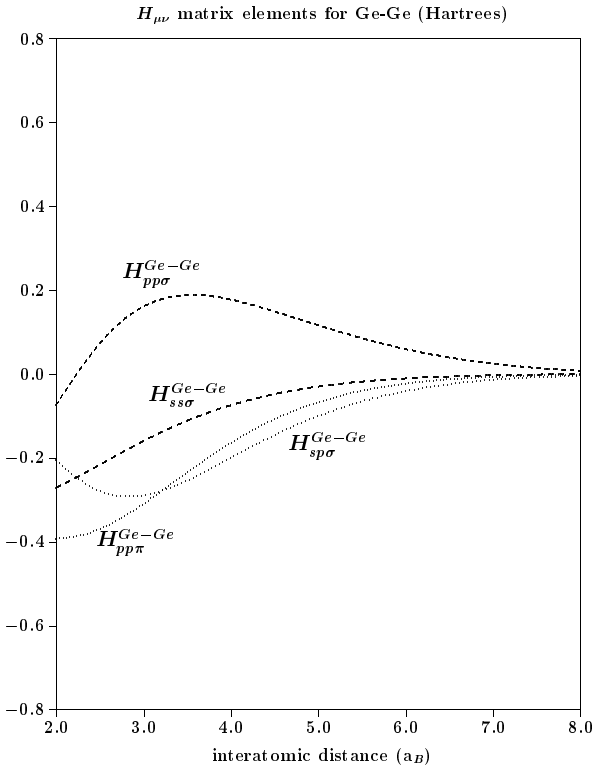

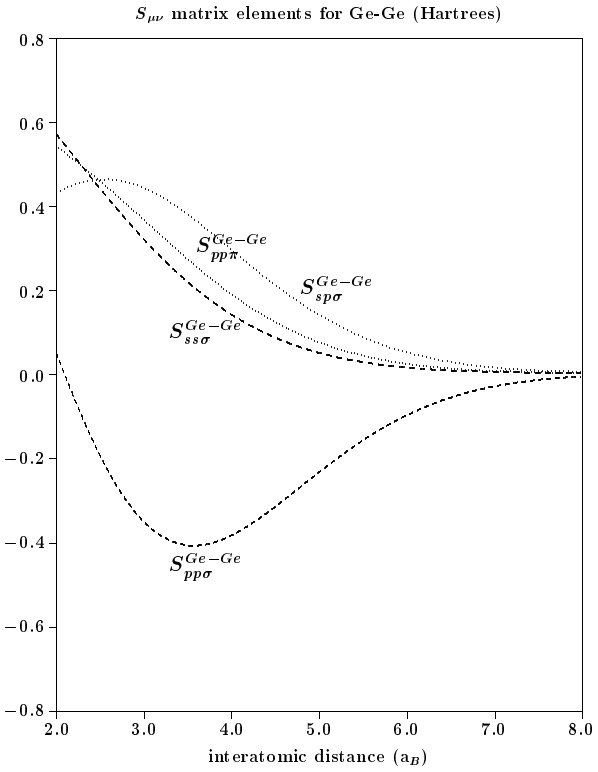

Figure 1. Hamiltonian and overlap matrix elements versus interatomic separation for (top) $H_{\mu\nu}$ and (bottom) $S_{\mu\nu}$ for Ge–Ge; and (top of the facing page) $H_{\mu\nu}$ and (bottom of the facing page) $S_{\mu\nu}$ for H–Ge, H–H. The interatomic separation is in Bohr radii; Hamiltonian matrix elements are in hartrees.

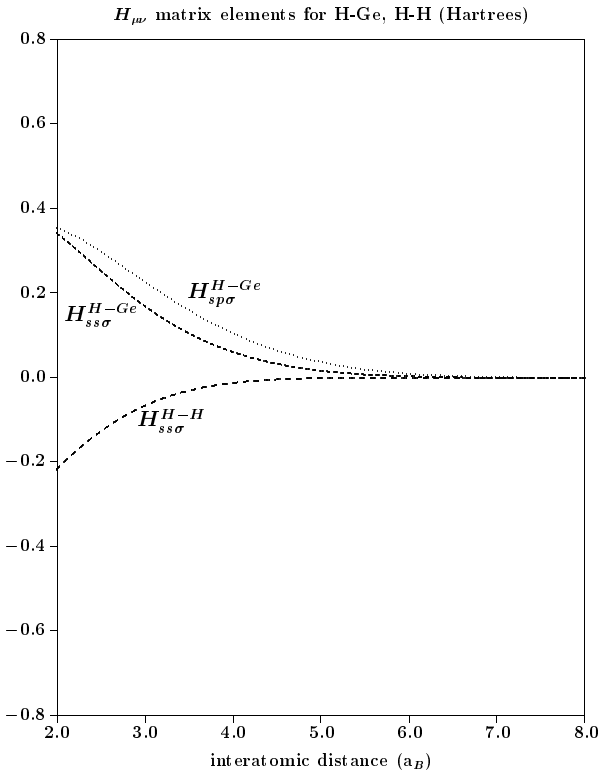

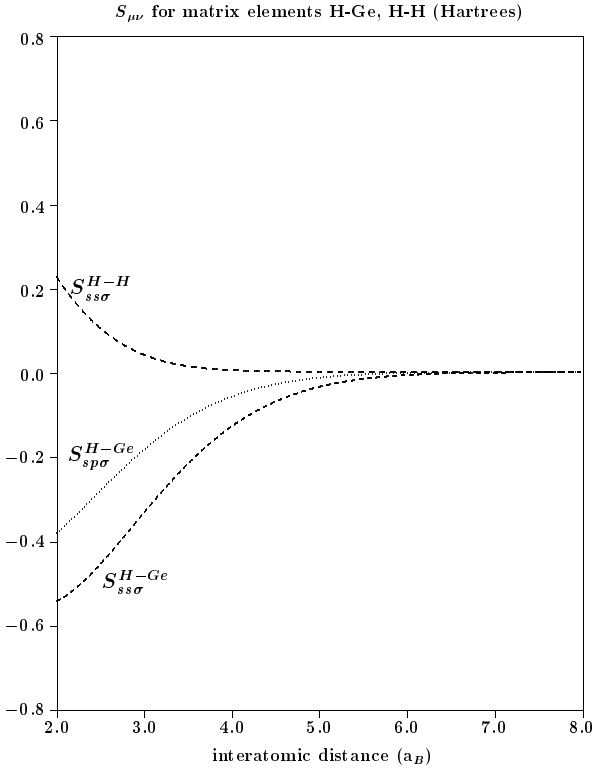

Figure 1. (Continued)

In our DF-TB approach we use a non-orthogonal overlap matrix and consider only two-centre Hamiltonian integrals, which are calculated using an LDA *ansatz*. Only a short-ranged repulsive two-particle potential still needs to be derived such that our total energies for small molecules and solids are equal to those of self-consistent calculations. Thus a very general description is obtained. This contrasts with other tight-binding methods for germanium [10, 11]. For example, in the work of Mercer and Chou [10], an orthogonal overlap matrix was considered and the tight-binding parameters were fitted to fourteen different tetrahedral volumes, giving a scaling ranging from $r^{-2.5}$ to $r^{-3.3}$.

This paper is arranged as follows. The application of the method to Ge and GeH is briefly described in section 2. Section 3 shows how the method has been tested against *ab initio* LDA results for small germanium clusters first generated in this paper. Section 4 describes the results for the solid phase, with a comparison of our derived (meta)stable phase diagram against that of experiment and SCF data [12], whilst section 5 discusses the results of our modelling of (100) surface reconstructions, both with and without hydrogen. Sections 6 and 7 are related to the Ge–H systems. Section 6 describes the comparison of our results for small Ge–H molecules against *ab initio* LDA results again first calculated in this paper. Our study of H defects in bulk Ge is described in section 7. Finally, section 8 gives a brief conclusion to the work.

2. Method

The DF-TB *ansatz* used in this work has been described in detail in other papers [7]. The method utilizes self-consistent LDF calculations for single atoms using a modified Kohn–Sham Hamiltonian to obtain atomic-like potentials and orbitals, $\phi_\nu(\boldsymbol{r} - \boldsymbol{R}_l)$. The modification in the single-atom potential takes the form of an additional term $(r/r_0)^2$ that confines the range of the atomic wavefunctions and charge density. The confining radius r_0 is related to the covalent radius of the atom type and does not involve fitting or parametrization. In a similar fashion to the pseudoatom construction for carbon [7] and silicon [8], we have used $r_0 = 2.12$ Å for germanium and $r_0 = 0.69$ Å for hydrogen. This is a well tested formulation based on the work of Seifert, Eschrig and Bieger [13, 14], who observed that this contraction in the atomic wavefunctions is characteristic of the effect when considering the many-atom case. The orbitals are then suitable as a minimal basis set for the expansion of the Kohn–Sham wavefunctions for the many-atom system:

$$\psi_i(\boldsymbol{r}) = \sum_\nu C_{\nu i}\phi_\nu(\boldsymbol{r} - \boldsymbol{R}_l). \tag{1}$$

Common to most tight-binding schemes, a two-centre approximation is used. Thus the overlap and Hamiltonian matrix elements, $S_{\mu\nu}$ and $H_{\mu\nu}$, are functions of interatomic separation only. They need therefore to be calculated only once for each pair of atom types (Ge–Ge, Ge–H, H–H) as a function of interatomic separation at a step width of 0.1 a_B up to the maximum interaction radius of 10 a_B. Beyond this distance the matrix elements are zero, due to the described contraction of the atomic orbitals. There is thus no need to explicitly impose a cut-off radius for the Hamiltonian and overlap matrix elements at, say, second-nearest-neighbour level as is done in most empirical tight-binding approaches. Our method also differs from these approaches in that we include non-orthogonality and all matrix elements are calculated in a parameter-free way from an atomic basis. Figure 1 shows the Hamiltonian and overlap matrix elements versus interatomic separation for Ge–Ge, H–Ge and H–H†.

† These Slater–Koster integrals are available in tabular form upon request from the authors.

The general eigenvalue problem

$$\sum_{\nu} C_{\nu i}(H_{\mu\nu} - \varepsilon_i S_{\mu\nu}) = 0 \tag{2}$$

is then solved non-self-consistently, in order to determine the single-particle energies, ϵ_i, and eigenstate expansion coefficients, $C_{\nu i}$, of the many-atom structure. Subsequently, the total energy is written as a sum of the 'band-structure energy', i.e. the sum of the energies of the occupied Kohn–Sham states, plus a repulsive two-body interaction term:

$$\begin{aligned} E_{tot}(\{\boldsymbol{R}_k\}) &= E_{BS}(\{\boldsymbol{R}_k\}) + E_{rep}(\{|\boldsymbol{R}_k - \boldsymbol{R}_l|\}) \\ &= \sum_i n_i \varepsilon_i(\{\boldsymbol{R}_k\}) + \sum_k \sum_{<l} V_{rep}(|\boldsymbol{R}_l - \boldsymbol{R}_k|). \end{aligned} \tag{3}$$

The short-range repulsive contributions $V_{rep}(R)$ can easily be determined as the difference of the cohesive energy resulting from self-consistent total energy calculations on molecular and crystalline reference systems [12] and the related band-structure energy, E_{BS}, for different values of inter-atomic distances R:

$$V_{rep}(R) = E^{scf}_{LDA}(R) - E_{BS}(R). \tag{4}$$

The interatomic force is then readily calculated:

$$F_{ij} = -\frac{\partial E_{tot}}{\partial R_{ij}} \tag{5}$$

where this represents the force on the ith atom in the j-direction. The atoms are then allowed to move under the influence of these forces to their minimum-energy positions.

For the work on small Ge clusters and Ge–H molecules, where neither experimental data nor self-consistent calculations exist in the literature, we have used the AIMPRO *ab initio* cluster program developed at Exeter by Jones and Briddon (see [15]). This utilizes a fully self-consistent pseudopotential density functional scheme together with wavefunctions expanded in Gaussian orbitals. This method has been successfully applied to a wide variety of systems ranging from small molecules to bulk materials with point and line defects [16, 17].

3. Small germanium clusters

In studying small germanium clusters, we compare principally to results generated from the self-consistent AIMPRO cluster program. The structures of Pacchioni and Koutecky [18] (PK), who have also investigated small germanium clusters of up to seven atoms using the self-consistent pseudopotential MO-LCAO scheme in combination with a configuration-interaction procedure, shall also be discussed. In addition, there are some empirical potential studies existing in the literature [19, 20]. We prefer not to consider these, as they tend to favour orderings of atoms found in the structures from which the potentials were derived. For example, the potential of Saito is specifically derived for sp^3 bonding. In consequence, many stable structures here are erroneously found to be distortions of the characteristic sixfold ring arrangement present in diamond.

Various high-symmetry arrangements have been considered by both the AIMPRO and the DF-TB method, which will be discussed in relation to the relevant cluster size. These structures are relaxed in the DF-TB approach using a stochastic MD quenching technique to obtain the transition path to the most stable clusters. Within the AIMPRO approach, all clusters are relaxed using conjugate gradients. In both the AIMPRO and DF-TB approaches,

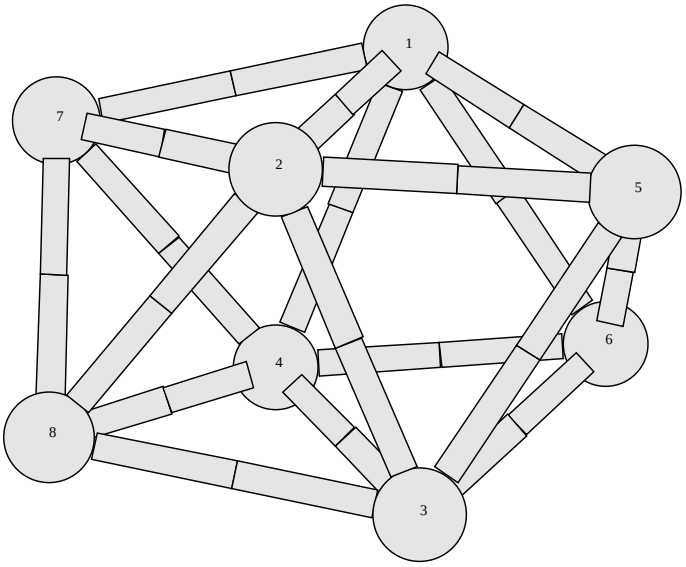

(a)

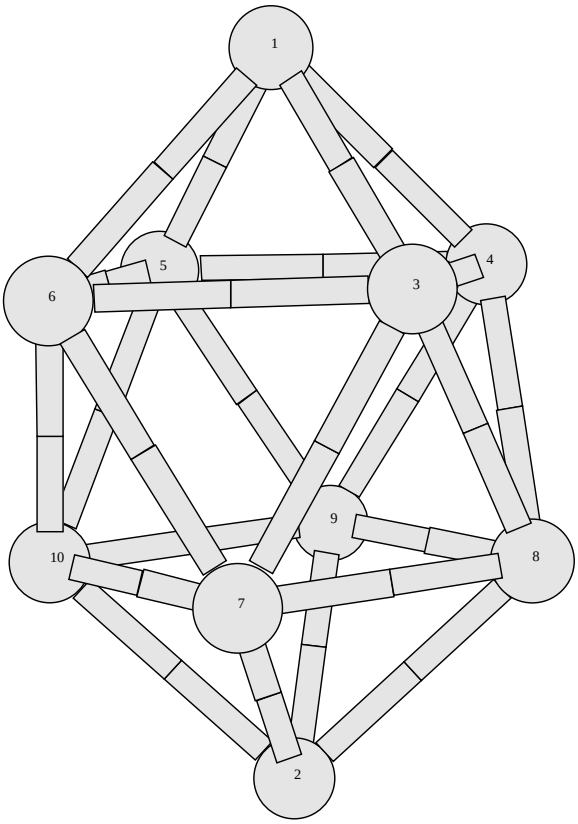

(b)

Figure 2. Minimum-energy structures found by the DF-TB method for (a) Ge_8 and (b) Ge_{10}.

Table 1. Optimized geometries for Ge_n clusters, $n = 2$–10. The column structure corresponds to the point group and figures in the articles cited. Bond lengths are in Å. For Ge_8 and Ge_{10} only the minimum-energy DF-TB structure is listed.

Cluster	Symmetry	Geometrical parameter	*Ab initio*	DF-TB
Ge_2	—	Ge_1–Ge_2	2.32	2.37
Ge_3	C_{2v}	Ge_1–Ge_2	2.26	2.33
		θ	78.5°	81.6°
Ge_4	D_{2h}	Ge_1–Ge_2	2.40	2.47
		Ge_1–Ge_3	2.40	2.47
Ge_5	C_{4v}	Ge_1–Ge_4	2.38	2.42
		Ge_1–Ge_2	2.54	2.41
		Ge_4–Ge_5	4.03	3.30
Ge_6	D_{4h}	Ge_1–Ge_2	2.48	2.50
		Ge_1–Ge_5	2.84	2.73
Ge_7	D_{5h}	Ge_1–Ge_3	2.59	2.60
		Ge_3–Ge_4	2.59	2.64
		Ge_1–Ge_2	2.72	2.91
Ge_8	C_2	Ge_1–Ge_2	—	2.67
	(figure 2(a))	Ge_2–Ge_3	—	2.67
		Ge_1–Ge_5	—	2.72
		Ge_2–Ge_5	—	2.54
		Ge_1–Ge_7	—	2.70
		Ge_2–Ge_7	—	2.60
Ge_9	C_{2v}	Ge_1–Ge_3	2.75	2.64
	(reference [21])	Ge_1–Ge_4	2.62	2.66
		Ge_2–Ge_3	2.56	2.60
		Ge_3–Ge_9	2.45	2.52
		Ge_4–Ge_7	2.70	2.70
Ge_{10}	D_{4d}	Ge_1–Ge_3		2.80
	(figure 2(b))	Ge_3–Ge_4		2.66
		Ge_3–Ge_7		2.65

all atoms are allowed to move freely under the forces acting upon them—no constraints are included to fix the atoms in certain high-symmetry positions.

A cursory glance at table 1 shows that for the minimum-energy configurations, the AIMPRO and DF-TB methods are in very good agreement for the structure geometries including their bond lengths and angles for all clusters except Ge_8 and Ge_{10}, where the stable clusters are found to have different symmetries. We shall discuss each cluster size in turn, mentioning also some metastable states found. We have, in addition, calculated the vibrational modes for all of the stable and metastable structures quoted to check that all of the modes are positive and hence the structures represent local energy minima on the potential energy surface for the clusters and are not metastable.

For Ge_3, in addition to the minimum-energy C_{2v} state, both methods find a metastable $D_{\infty h}$ structure i.e. a linear chain configuration 0.69 eV higher in energy in the DF-TB method and 0.40 eV higher in the AIMPRO method. There is agreement that the D_{3h} structure is unstable.

The Ge_4 minimum-energy D_{2h} structure is augmented by metastable D_{4h} and T_d states at energies 1.0 and 0.8 eV higher than the ground state respectively by the DF-TB method, and 3.0 and 1.90 eV by the AIMPRO method. The D_{2h} minimum-energy structure has bond length 2.41 Å in the DF-TB compared with 2.40 Å in the AIMPRO method, with the internal angles being 56.53° and 53.0° respectively. These minimum-energy Ge_3 and Ge_4

structures are also those of PK.

Moving on to the Ge_5 case, the AIMPRO and DF-TB methods again agree on the minimum-energy C_{4v} configuration. This contrasts with the results of PK, who report a D_{3h} structure. We find this to be unstable when relaxed by both the DF-TB and AIMPRO methods. Additionally, we obtain a C_{2v} state lying 1.63 eV higher in energy within the DF-TB method and 0.62 eV within the AIMPRO method.

For the Ge_6 structure, both the AIMPRO method and the DF-TB method predict a D_{4h} state. PK find an O_h structure, which is unstable in the DF-TB method. In addition, we determine the D_{3d} and C_{2v} states to be unstable in both methods, transforming spontaneously to the minimum-energy structure.

For the larger clusters, Ge_7–Ge_{10}, we have used the symmetries found to be stable for the corresponding silicon clusters by the DF-TB method [8] as our starting structures. However, we have relaxed these clusters by using a stochastic annealing regime. As a result, Ge_7 forms a stable D_{5h} structure by both methods. We were unable to find any further metastable states for this cluster.

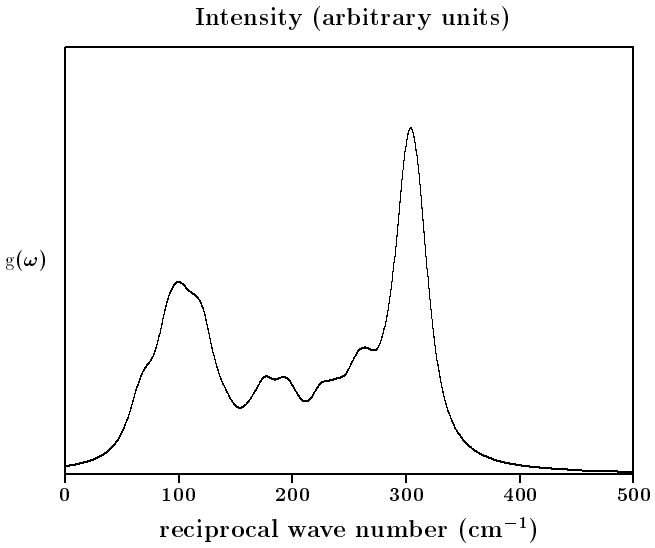

Figure 3. The phonon density of states for germanium. This is expressed as intensity (arbitrary units) versus frequency (cm^{-1}).

For the eight-atom cluster, the DF-TB method determines a C_2 symmetry structure shown in figure 2(a) to be that of minimum energy. The geometry is a distorted octahedron with two adjacent faces capped and is also reported by Frauenheim *et al* [8] to be the lowest-energy Si_8 cluster. For Ge, we additionally obtain a C_S edge-capped pentagonal bipyramid described by Raghavachari (see [21]) to lie higher in energy by only 0.02 eV and a distorted C_{2v} face-capped pentagonal bipyramid 0.45 eV higher in energy (figures 8(f) and 8(e) respectively in Raghavachari and Rolfing's paper [21]). The AIMPRO method yields a different energetic ordering. Whilst all of the above-mentioned structures above represent local minima, the C_{2v} face-capped pentagonal bipyramidal is the ground state followed energetically by the C_S edge-capped pentagonal bipyramid and the distorted bicapped C_2 octahedron lying at 0.08 and 0.29 eV, respectively.

In the Ge_9 case, we find the AIMPRO and DF-TB methods in agreement that the

tricapped distorted prism with C_{2v} symmetry suggested by Ordejón *et al* [22] for silicon is the most stable structure for Ge. As for silicon, a distorted tricapped octahedron is metastable at 1.4 and 1.5 eV higher in energy within the AIMPRO and DF-TB methods respectively.

For the Ge_{10} clusters, we disagree with DF-TB work on Si, where a tetracapped trigonal prism with C_{3v} symmetry was established to be the minimum-energy structure. We find with the DF-TB method that the bicapped tetragonal anti-prism with D_{4d} symmetry, shown in figure 2(b), is the most stable. In addition, a tetracapped octahedron with T_d symmetry described by Raghavachari (see [21]) for Si_{10} is metastable, with energy at 1.66 eV above the ground state. The AIMPRO method also finds both of these structures to be stable, however with reverse energetic ordering, the T_d state being 0.3 eV lower in energy.

4. The bulk phase

Yin and Cohen [12] have performed accurate self-consistent LDF supercell calculations of the cohesive energies of various crystalline forms of germanium. The reproduction of their results is a necessary benchmark of the validity of our DF-TB scheme.

Table 2. Predictions of the bulk properties of the diamond, body-centred cubic, BCC, face-centred cubic, FCC, and simple cubic, SC, lattices as compared to the *ab initio* pseudopotential results of Yin and Cohen.

Crystal	Theoretical method	Nearest-neighbour distance (Å)	Relative energy per atom (eV/atom)
Diamond	DF-TB	2.45	0.0
	Yin and Cohen	2.45	0.0
SC	DF-TB	2.67	+ 0.26
	Yin and Cohen	2.66	+ 0.31
BCC	DF-TB	2.79	+ 0.41
	Yin and Cohen	2.86	+ 0.44
FCC	DF-TB	2.87	+ 0.50
	Yin and Cohen	2.96	+ 0.46

For each of the crystalline phases, the total energy of a supercell is calculated within the DF-TB method as a function of the nearest-neighbour distance. The cohesive energy per atom can then be found versus the interatomic separation and thus the phase diagram for germanium can be obtained. Table 2 gives a comparison of the results found in this work with those of Yin and Cohen.

The results show that the DF-TB method correctly predicts the diamond form to be the stable crystalline structure and that there is exact agreement between the DF-TB and Yin and Cohen methods for the interatomic distance in the diamond lattice. Furthermore, we find an energy per atom of 5.01 eV in comparison with a value of 4.26 eV/atom given by Yin and Cohen. Taking into account that our calculations are done without spin polarization which will reduce the difference between these results, this is a reasonable agreement. The bulk modulus is found to be 0.77 MBar, in exact agreement with experimental results [23]. We can therefore be sure that our data well describe the bulk diamond phase. Furthermore, as the table shows, there is excellent agreement between the two methods for the minimum-energy interatomic bond lengths in simple cubic, SC, bond-centred cubic, BCC, and face-centred cubic, FCC, structures, the percentage differences between the two methods being 0.4%, 2.5% and 3.0% respectively. The relative stabilities of the various crystalline phases are

also correctly reproduced in the sequence diamond, SC, BCC and FCC, with errors per atom of 0.05, 0.03, 0.04 eV for SC, BCC and FCC respectively in comparison with the results of Yin and Cohen.

Additionally, we have calculated the band structure of the diamond phase, where we find the valence bands to be well described by our approach. However, the conduction band states are not well represented, resulting in the prediction of a direct band gap and an overestimate, at 0.93 eV, of its size. Grosso (see [11]), in his tight-binding formalism, finds this to be due to the neglect of second-nearest-neighbour terms and reports that their inclusion remedies this problem. This cannot be the case here, as, as the discussion in section 2 indicated, these are included in our calculations.

The discrepancy comes from the use of a minimal basis in the wavefunction expansion. An spd or sps* hybridized basis set would firstly be expected to narrow the gap between occupied and unoccupied states, due to the admixture of additional d or s* states. Moreover, this admixture will be dependent on the $\boldsymbol{k}$-vector, thus altering the relative positions of the conduction band minima and valence band maxima.

We have also calculated the vibrational spectrum for the bulk diamond phase by the standard method of diagonalizing the dynamical matrix within the harmonic approximation [24]. The calculated spectrum has been convoluted by the experimental resolution function and is displayed in figure 3. We find the most characteristic modes with appropriate intensities at the correct wavenumbers and the overall width of the vibrational spectrum to be in good agreement with the existing theoretical and experimental data [25, 26].

5. Reconstruction of the (100) germanium surface

The structure of clean germanium (100) surfaces has been extensively investigated both experimentally [27, 28] and theoretically [29, 30, 31]. LEED studies by Kevan [28] predict an asymmetric (4×2) reconstruction at low temperatures. Tunnelling microscopy experiments by Kubby *et al* [27] show islands of (2×1), (2×2) and (4×2) reconstructions on the Ge surface at room temperature. Needels *et al* [29], using a self-consistent plane-wave pseudopotential method, found the (4×2) and (2×2) reconstructions to have the lowest energy and to be almost degenerate in energy.

Spiess *et al* [30] using an *ab initio* cluster method, confirm the (2×2) and (4×2) reconstructions with lowest energy. The asymmetric (2×1) reconstruction is, however, determined to be very close in energy. The details of the exact geometry of the (4×2) reconstruction differ between the two groups. Nevertheless, both agree that the Ge–Ge dimer bond is weaker than the corresponding bulk bond. Spiess *et al* give 2.50 Å compared to 2.48 Å from Needels *et al*.

Table 3. A comparison of DF-TB results for the various reconstructions at a Ge(100) surface.

Configuration	Ge–Ge dimer bond length (Å)	Tilt angle	Energy per dimer (eV)
(2 × 2)	2.51	19.2°	0.00
(4 × 2)	2.51	19.2°	+ 0.01
(2 × 1)	2.51	17.6°	+ 0.05

We have relaxed a 216-atom supercell using a conjugate-gradient technique within the DF-TB scheme. The supercell is displayed in figure 4. It consists of seven layers of

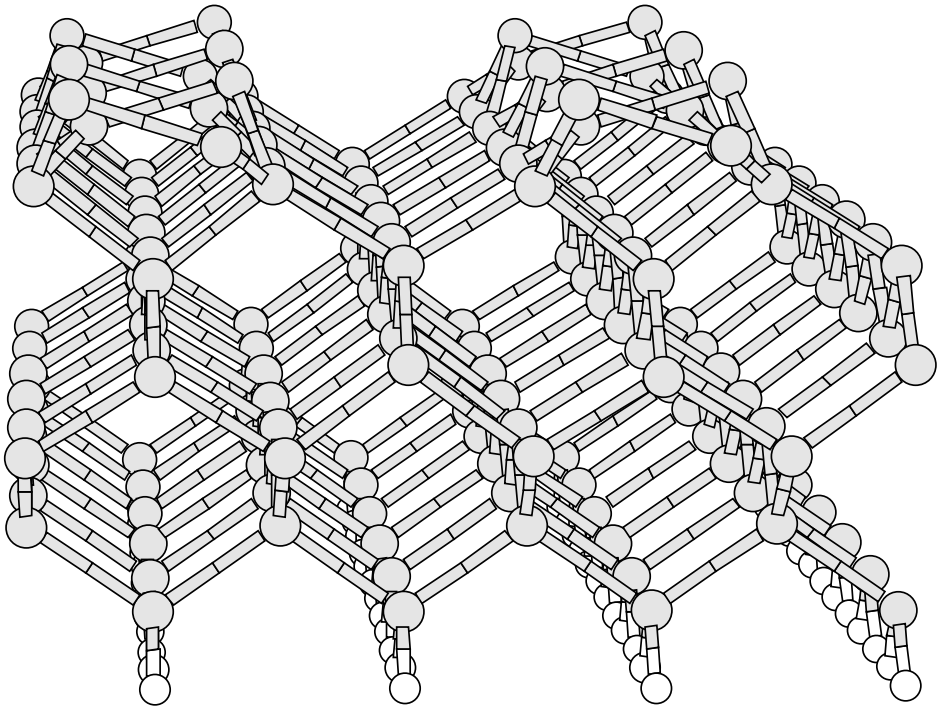

Figure 4. The 216-atom supercell displaying the 2×2 reconstructed (100) surface of germanium.

germanium atoms, with the dangling bonds on the lowermost layer terminated by hydrogen atoms. There are 24 atoms on the uppermost surface. During relaxation, the lowest two germanium layers plus the terminating hydrogen atoms are held fixed to simulate the bulk. Although the (2×1), (2×2) and (4×2) symmetries are imposed as starting configurations, the surface atoms are not constrained to remain in their initial high-symmetry arrangements; they are free to explore the (100) surface. Our results are shown summarized in table 3. In all cases, the reconstruction symmetry is found to be stable. Energies are quoted relative to that of the (2×2) reconstruction, as we find this to have the lowest energy. It can be seen that there is good agreement with the other theoretical studies. The (2×2) structure is lowest in energy, with the (4×2) structure lying only slightly higher at $+0.01$ eV/dimer and the (2×1) reconstruction at $+0.05$ eV/dimer. This is consistent with the results obtained by other theoretical groups and the experimental observation that the three states coexist at room temperature. There is also excellent agreement as to the dimer bond length: 2.51 Å by the DF-TB method as compared to 2.48 and 2.50 Å from the *ab initio* methods.

Since hydrogen is expected to play an integral role in the CVD growth of germanium, due to the presence of GeH_4, we have terminated the (2×2) surface with hydrogen. After a conjugate-gradient relaxation, the resulting structure is a flat reconstructed (100) surface with the buckling removed. This is what one would expect as the Ge dangling bonds are removed by the hydrogen termination. The Ge–H and Ge–Ge bond lengths are 1.54 Å and 2.45 Å respectively, almost exactly those of bulk Ge–Ge bonds and the Ge–H bond in GeH_4 respectively (see the next section). The Ge atoms to which the hydrogen atoms are attached are relaxed back into the surface by 0.15 Å. The energy gain for tying off a dangling bond on Ge(111) is 0.38 eV.

6. Germanium–hydrogen molecules

We now describe results which utilize our Ge–H data on small Ge–H molecules.

We again make use of a stochastic MD quenching technique to relax the various molecules, with all of the atoms allowed to move freely to their minimum-energy positions. The results for molecules GeH, GeH_2, GeH_4, Ge_2H_6, Ge_3H_8 and Ge_6H_{12} are shown in table 4, in comparison with AIMPRO results and experimental findings [32]. As can be seen, the geometries, bond lengths and bond angles show good agreement between the self-consistent calculations, experimental data and our DF-TB results. There is one exception, however: the Ge–Ge–Ge angle in the Ge_3H_8 case on which AIMPRO and DF-TB results differ considerably. We have therefore re-relaxed the AIMPRO structure without symmetry constraints using an all-electron, full potential Gaussian orbital cluster code [33]. We find the Ge–Ge–Ge angle to be 114.1° with Ge–Ge bond lengths of 2.40 Å and Ge–H lengths 1.54 Å in excellent agreement with the DF-TB results. It is postulated that a larger basis is required for the electronic wavefunction expansion in this case for the AIMPRO method.

For the Ge_6H_{12} ring structure, both methods agree that a slightly buckled chair structure is stable with bond lengths of 116.5° for the DF-TB method and 117.0° for the AIMPRO method respectively. The DF-TB method finds a flat ring to be metastable in energy. Within the AIMPRO method, this is found to be unstable, relaxing to the chair form. To summarize, the DF-TB method gives reliable results for the structures of small Ge–H molecules, modelling accurately their bond lengths and angles.

7. Hydrogen in bulk germanium

7.1. Single hydrogen defects in germanium

Isolated hydrogen is a commonly occurring defect in semiconductors. Its presence in diamond and silicon in particular has been extensively investigated, both theoretically and experimentally. For a review, the reader is referred to Van de Walle's paper [34]. It is found that in both cases the stable site for a single hydrogen atom is the so-called bond-centred site (H_{bc}). This is a point midway between two bonding host atoms. In addition, there are metastable states associated with the high-symmetry tetrahedral (H_{tet}) and anti-bonding (H_{ab}) sites. The only existing theoretical calculations for Ge are those of Estreicher and Maric [35], who used an *ab initio* Hartree–Fock method. However, these studies were undertaken using a small cluster of only fourteen host atoms with dangling bonds saturated by hydrogen atoms. In some cases no lattice relaxations have been allowed. They found that, in contrast to the cases of silicon and diamond, the stable site for an isolated H atom is the tetrahedral site. The anti-bonding site is determined to be nearly degenerate in energy, with the bond-centred site lying higher in energy. Their reasoning for these results is as follows: the stability of the tetrahedral (T) site increases with lattice constant as the energy of H_{tet} converges towards H_{free}. In contrast, the stability of H_{bc} is governed principally by two factors. The first factor is the strength of the H–host bond, a strong bond stabilizing the defect site. This is optimized for C and weakens in the series C, Si, Ge. The second factor is that of the 'lattice size effect', the ability of the lattice to accommodate the relaxation involved in the formation of an optimal bridging bond. This, they reasoned, is optimized for Si. The combination of these factors results in the bond-centred site being higher in energy than the anti-bonding and tetrahedral sites for Ge. Muon spin rotation studies support their findings [36, 37].

Our calculations have been carried out by inserting hydrogen atoms into a 216-atom

Table 4. A comparison of the structures of small germanium–hydrogen clusters obtained from DF-TB and AIMPRO relaxations.

Molecule	Method	Ge–Ge bond length (Å)	Ge–H bond length (Å)	Ge–Ge–Ge bond angle	H–Ge–H bond angle
GeH	DF-TB	—	1.61	—	—
	AIMPRO	—	1.61	—	—
	Experiment [32]	—	1.67	—	—
GeH_2	DF-TB	—	1.59	—	92.0°
	AIMPRO	—	1.60	—	92.1°
GeH_4	DF-TB	—	1.51	—	109.5°
	AIMPRO	—	1.54	—	109.5°
Ge_2H_6	DF-TB	2.35	1.52	—	106.3°
	AIMPRO	2.46	1.56	—	113.0°
	Experiment	2.41	1.50	—	—
Ge_3H_8	DF-TB	2.40	1.52	116.5°	—
	AIMPRO	2.46	1.56	95.0°	—
	Experiment	2.41	1.50	—	—
Ge_6H_{12}	DF-TB	2.37	1.53	116.5°	102.0°
	AIMPRO	2.51	1.55	117.0°	101.3°

Table 5. The energetic stabilities of single isolated hydrogen atoms in the germanium diamond lattice as calculated by the DF-TB method.

Position in lattice	Bond length H–Ge	Energy (eV)
H_{tet}	2.56 (×4)	0.00
H_{ab}	1.61	+ 0.08
H_{bc}	1.60 (×2)	+ 0.93

diamond supercell at the bond-centred, tetrahedral and anti-bonding sites and relaxing the resultant clusters using a conjugate-gradient technique. The atoms were not constrained to remain 'on-site'; rather they were allowed to relax freely without constraints fixing them at high-symmetry positions. All sites, however, were found to be (meta)stable. The relative energies and bond lengths for H_{bc}, H_{ab}, H_{tet} are given in table 5. The results are quoted relative to the energy of the tetrahedral site, as this is found to have the lowest energy. It can be seen that the energetic ordering of the defects corresponds to that of Estreicher. The H_{tet} atom remains in an on-site position equidistant from four Ge atoms. The H_{ab} site has a shortish bond of 1.61 Å to one host atom, with the Ge atom to which the H_{ab} is bonded moving into the plane of three of its nearest neighbours and a distance 3.0 Å from the fourth. Thus it forms three sp^2-like bonds with its in-plane neighbours and one p-type bond with H_{ab}. However, in accordance with Estreicher's prediction, we find this state to be almost degenerate with the H_{tet} site.

H_{bc} has the highest energy of all of the defects, with the two Ge atoms to which it is bonded moving outwards causing some lattice relaxation. Their Ge–Ge back-bonds, however, are not appreciably strained, shortening them by less than 2%.

With regard to the electronic states of these defects, we find that the bond-centred defect has a partially filled level occurring in the upper half of the band gap, 0.2 eV from the conduction band edge. For the anti-bonding and tetrahedral defects, a single level is seen below mid-gap, 0.2 eV and 0.05 eV above the valence band top for the anti-bonding and tetrahedral defects respectively. With these results, we confirm the predictions of Estreicher

and Maric and present moreover the first calculations performed on these defects using such a large supercell and with full lattice relaxation of all of the defects.

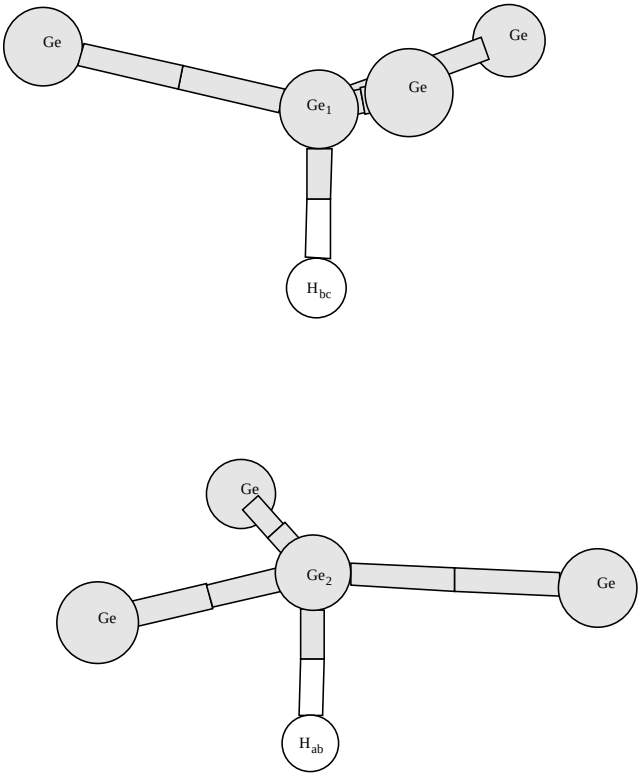

Figure 5. The H_2^* defect.

7.2. Hydrogen pairs in germanium

Finally, we have also investigated the structure of pairs of hydrogen atoms in Ge, in particular the H_2^* defect. This is the stable form of H_2 in carbon [38] and is found to be metastable in silicon [39]. It has also been recently investigated in germanium by Bech Nielsen *et al* (see [40]). It consists of two interstitial hydrogen defects, one at a bond-centred site H_{bc} between two germanium atoms, Ge_1 and Ge_2, and a second H atom at the corresponding anti-bonding site H_{ab} (see figure 5). The *ab initio* calculations for the H_2^* in germanium show that the H_{bc} moves slightly towards one of the germanium atoms, Ge_1, and forms a bond of length 1.52 Å. H_{ab} moves to a near tetrahedral site, taking Ge_2 with it, thus forming a bond of length 1.60 Å.

We have applied our DF-TB approach for Ge–Ge and Ge–H in order to compare with these results. Again, the 216-atom supercell was used and two H atoms were added. This was again relaxed using a conjugate-gradient technique, with the H atoms not constrained to sit on-site. When relaxed, our defect has a similar geometry to the *ab initio* structure; the Ge_1–Ge_2 bond is effectively broken, with the two atoms 4.01 Å apart. The H_{bc} atom forms a short, strong bond of 1.49 Å with Ge_1 and likewise the H_{ab} atom forms a strong, short bond of 1.53 Å with Ge_2. The Ge_2 also relaxes into a planar sp^2-like bonding arrangement.

The bond lengths obtained are shorter than the corresponding cases for single, isolated H defects. This is to be expected, as for the single-H case there is still some residual Ge–Ge bonding; hence the H atom must 'share' the host Ge atom with another Ge atom, thus weakening and lengthening the Ge–H bond. The H_2^* defect has an associated filled state just above the valence band top in accordance with the *ab initio* prediction. Thus the DF-TB method is shown to accurately model hydrogen defect complexes in Ge.

8. Conclusion

In summary, we have derived a density functional non-orthogonal tight-binding approach for Ge and Ge–H which is based on an LCAO approach using a two-centre integral approximation scheme. We have applied this formalism to various-scale Ge and Ge–H structures and compared our results with existing experimental and theoretical data and some further data generated using the AIMPRO density functional self-consistent cluster program. We have shown good agreement for small germanium clusters, germanium–hydrogen molecules, crystalline germanium and both hydrogenated and unhydrogenated germanium (100) surfaces. In addition, we have performed calculations for single hydrogen atoms in crystalline Ge. These are the first calculations of this type done on Ge using large fully optimized supercells and confirm self-consistent *ab initio* calculations done on small clusters. Further, we have calculated the structure of the so-called H_2^* defect and compared to existing SCF cluster calculations, finding very good agreement.

Thus we have demonstrated that the density-functional-based tight-binding molecular dynamics method is efficient and accurate for germanium–hydrogen systems. We intend in the future to use this formalism to study complex Ge–H systems such as a-Ge:H.

Acknowledgment

The support of the Deutsche Forschungsgemeinshaft is gratefully acknowledged.

References

[1] Nelmes R J, McMahon M I, Wright N G, Allen D R and Loveday J S 1993 *Phys. Rev.* B **48** 9883
[2] Mujica A and Needs R J 1993 *Phys. Rev.* B **48** 17 010
[3] Takeuchi N and Garzon I L 1994 *Phys. Rev.* B **50** 8342
[4] Kresse G and Hafner J 1994 *Phys. Rev.* B **49** 14 251
[5] Ding K and Andersen H C 1986 *Phys. Rev.* B **34** 6987
[6] Plättner R, Günzel E, Schneinbacher G and Schröder B 1991 *AIP Conf. Proc.* **234**
[7] Porezag D, Frauenheim T, Köhler T, Seifert G and Kaschner R 1995 *Phys. Rev.* B **51** 12 947
[8] Frauenheim T, Weich F, Köhler T, Porezag D and Seifert G 1995 *Phys. Rev.* B **52** 11 492
[9] Widany J, Frauenheim T, Köhler T, Sternberg M, Jungnickel G and Seifert G 1996 *Phys. Rev.* B **53** 4443
[10] Mercer J L and Chou M Y 1993 *Phys. Rev.* B **47** 9366
[11] Grosso G and Piermarocchi C 1995 *Phys. Rev.* B **51** 16 772
[12] Yin M T and Cohen M L 1982 *Phys. Rev.* B **26** 5668
[13] Seifert G and Eschrig H 1985 *Phys. Status Solidi* b **127** 573
[14] Seifert G, Eschrig H and Bieger W 1986 *Z. Phys. Chem., Lpz.* **267** 529
[15] Jones R 1992 *Phil. Trans. R. Soc.* A **341** 157
[16] Briddon P R and Jones R 1993 *Physica* B **185** 179
[17] Sitch P, Jones R, Öberg S and Heggie M I 1994 *Phys. Rev.* B **50** 17 717
[18] Pacchioni G and Koutecky J 1986 *J. Chem. Phys.* **84** 3301
[19] Antonio G A, Feulso B P, Kalia R K and Vashishta P 1988 *J. Chem. Phys.* **88** 7671
[20] Saito S, Ohnishi S and Sugano S 1986 *Phys. Rev.* B **33** 7036
[21] Raghavachari K and Rolfing C M 1988 *J. Chem. Phys.* **89** 2219

[22] Ordejón P J, Lebedenko D and Menon M 1994 *Phys. Rev.* B **50** 5645
[23] McSkimin H J 1953 *J. Appl. Phys.* **24** 988
[24] Köhler T, Frauenheim T and Jungnickel G 1995 *Phys. Rev.* B **52** 11 837
[25] Srivastava G P 1981 *Phys. Rev.* B **25** 2815
[26] Nelin G and Nilsson G 1971 *Phys. Rev.* B **5** 3151
[27] Kubby J A, Griffith J E, Becker R S and Vicker J S 1987 *Phys. Rev.* B **36** 6079
[28] Kevan S D 1985 *Phys. Rev.* B **32** 2344
[29] Needels M, Payne M C and Joannopoulus J D 1988 *Phys. Rev.* B **38** 5543
[30] Spiess J A, Freeman A J and Soukiassian P 1994 *Phys. Rev.* B **50** 2 249
[31] Krüger P 1991 *Adv. Solid State Phys.* **31** 133
[32] 1976 *Gmelin Handbook of Inorganic Chemistry* vol 45 (Köln: TÜV Rheinland) p 31
[33] Pederson M R and Jackson K A 1991 *Phys. Rev.* B **43** 7312
[34] Van de Walle C G 1991 *Physica* B **170** 21
[35] Estreicher S K and Maric Dj M 1993 *Phys. Rev. Lett.* **70** 3963
[36] Patterson B D 1988 *Rev. Mod. Phys.* **60** 3966
[37] Lichti R L, Lamp C D, Kreitzmann S R, Kiefli R F, Schneider J W, Niedermayer C, Chow K, Pfiz T, Estle T L, Dodds S A, Hitt B and DuVarney R C 1992 *Mater. Sci. Forum* **83–87** 1115
[38] Briddon P, Jones R and Lister G M S 1988 *J. Phys. C: Solid State Phys.* **21** L1027
[39] Holbech J D, Bech Nielsen B, Jones R, Sitch P and Öberg S 1993 *Phys. Rev. Lett.* **71** 875
[40] Bech Nielsen B, Hoffmann L, Jones R and Öberg S 1995 *Mater. Sci. Forum* **196** 879